Simultaneous inversion of magnetic data into induced and remanent magnetizations

Introduction

Traditional TMI data inversion methods operate under the assumption that rocks lack remanent magnetization, attributing the observed magnetic field solely to induced magnetization. These methods aim to invert for magnetic susceptibility, which links induced magnetization to the Earth's magnetic field. However, rocks exhibit both induced and remanent magnetizations, preserving the historical Earth's magnetic field at the time of their formation. Two primary natural mechanisms contribute to remanent magnetization. Firstly, in igneous rocks, as magnetic minerals cool through the Curie point, their magnetic domains align with the Earth's magnetic field during formation, preserving a permanent record of orientation. The second mechanism occurs during sedimentation, where tiny grains in sedimentary deposits align with the Earth's magnetic field during deposition before the rock consolidates.

Efforts to extract remanent magnetization from observed TMI data have gained significant attention in research and applications in recent decades (e.g., Ellis et al., 2012; Zhu et al., 2015; Li, 2017; Jorgensen and Zhdanov, 2021; Jorgensen et al., 2023). Many developed methods focus on inverting TMI data into the distribution of the magnetization vector underground. This vector, obtained via inversion, is then separated into remanent and induced magnetizations using various approximations.

In our current study, we adopt a rigorous approach by simultaneously inverting TMI data into the induced and remanent components of the magnetization vector. To mitigate the non-uniqueness of the inverse problem, we employ Gramian regularization (Zhu et al., 2015; Jorgensen and Zhdanov, 2021). Our demonstration indicates that this methodology offers a robust means of identifying remanent magnetization from observed TMI data.

Theory

In a general case, the total magnetization vector, $\mathbf{M}$ can be represented as a superposition of induced, $\mathbf{M}_{ind}$, and remanent, $\mathbf{M}_{rem}$, magnetizations:

$\mathbf{M}(\boldsymbol{r}) = \mathbf{M}_{ind}(\boldsymbol{r}) + \mathbf{M}_{rem}(\boldsymbol{r}), \quad \mathbf{M}_{ind}(\boldsymbol{r}) = \chi(\boldsymbol{r})\mathbf{H}_0,$ and $\mathbf{M}_{rem}(\boldsymbol{r}) = \{R_x(\boldsymbol{r}), R_y(\boldsymbol{r}), R_z(\boldsymbol{r})\},$

where $\chi(\boldsymbol{r})$ is the magnetic susceptibility, $\mathbf{H}_0$ is the inducing magnetic field, and $\{R_x(\boldsymbol{r}), R_y(\boldsymbol{r}), R_z(\boldsymbol{r})\}$ are the scalar components of the remanent magnetization.

Our goal is to determine magnetic susceptibility and remanent magnetization simultaneously. This inverse problem presents a formidable challenge due to the presence of four unknown scalar parameters for each cell, rendering the problem ill-posed. Addressing this challenge involves regularization using Gramian constraints and a smoothness term based on susceptibility.

The works by Zhu et al. (2015) and Jorgensen and Zhdanov (2021) demonstrated the feasibility of achieving a reliable solution to the inverse problem concerning the magnetization vector through the reinforcement of correlations among its different components. We propose employing this supplementary constraint specifically on the components of the remanent magnetization. This can be accomplished by minimizing the Gramian stabilizers,

$$S_G(\boldsymbol{m}) = \begin{vmatrix} (\boldsymbol{R}_\beta, \boldsymbol{R}_\beta) & (\boldsymbol{R}_\beta, \boldsymbol{\chi}) \\ (\boldsymbol{\chi}, \boldsymbol{R}_\beta) & (\boldsymbol{\chi}, \boldsymbol{\chi}) \end{vmatrix}, \beta = x, y, z;$$

where $\boldsymbol{R}_\beta$ is the vector of the β component of remanent magnetization, and $\boldsymbol{\chi}$ is the vector of magnetic susceptibility formed by their values in every cell. In order to reduce the ambiguity related to the contribution of the induced and remanent magnetization in the total field, we can incorporate in the inversion some a priori information about the magnetic susceptibility, $\boldsymbol{\chi}_{apr}$. This can be achieved by imposing the following constraint:

$$S_\chi(\boldsymbol{m}) = \|\boldsymbol{\chi} - \boldsymbol{\chi}_{apr}\|^2.$$

Thus, the parametric functional for the regularized solution of the inverse problem takes the following form:

$$P^{\alpha}(\boldsymbol{m}) = \phi(\boldsymbol{m}) + \alpha c_1 S_{\chi}(\boldsymbol{m}) + \alpha c_2 \sum_{\beta=x,y,z} S_G(\boldsymbol{m}) = min,$$

where $\phi(\boldsymbol{m})$ is a data misfit term, α is a regularization term, and c_1, c_2 balance the stabilizers. The parametric functional is minimized using a reweighted regularized conjugate gradient scheme (Zhdanov, 2015). If no a priori susceptibility information is known in the area, $\boldsymbol{\chi}_{apr}$ is determined by inversion for susceptibility alone and used as a soft constraint.

Example using synthetic data

The algorithm's efficacy was evaluated using two synthetic models: one featuring a prism solely susceptible and another with susceptibility and remanent magnetization. These prisms were identical in size, measuring 400 meters on each side and 100 meters in thickness, buried at a depth of 100 meters below the surface. Synthetic data was generated with a magnetic susceptibility of 0.1 SI for both cases. In the second scenario, the model included a remanent magnetization of 0.1 A/m in magnitude, inclined at 45°, and declinated at 35°. Both cases were simulated under an inducing field with a total field strength of 50,000 nT, inclined at 75°, and declinated at 5°. During the inversions, initial stabilizer values (α) and weights (c_1, c_2) were set to one. Additionally, a minimum error floor of 0.01 nT was assumed, and the iterative process ceased upon reaching a 5% data misfit.
The developed method's inherent capability to discern between induced and remanent magnetization is quite remarkable. Figure 1 corresponds to the synthetic model, which is purely susceptible with no remanent component and shows horizontal slices of the various magnetic models at a depth of 180 m below the surface. A well-defined body is recovered in the induced magnetization; however, only weak remanence is observed. We contrast this to Figure 2, which corresponds to the synthetic model with both induced and remanent components and shows horizontal sections of the magnetic models at the same depth as Figure 1. We can see the method's capability to recover remanence when it exists successfully and the converse–only weak remanence is recovered when none exists. This is impressive, considering no advanced weighting was required in the balancing of the various stabilizing terms. The inversions were all run with initial regularization terms of unity.

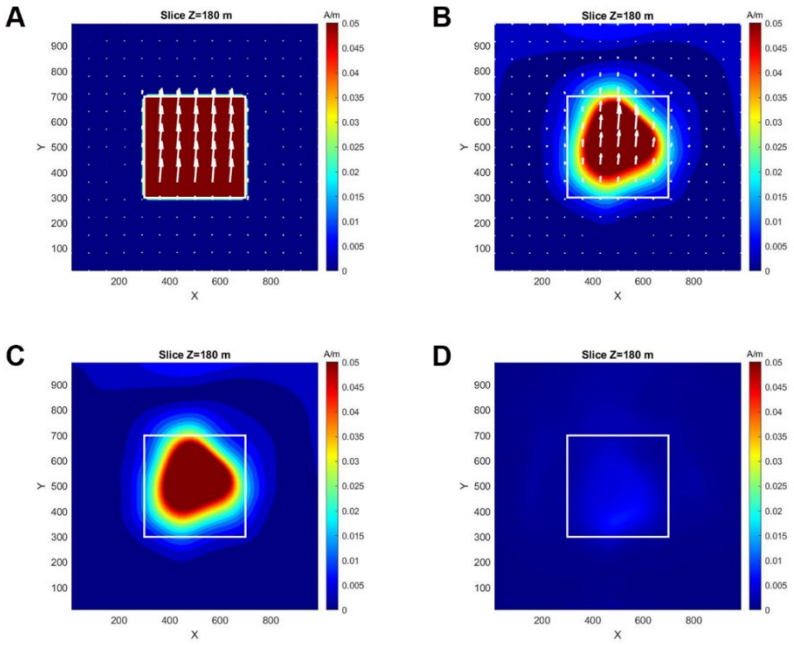

Figure 1 *Horizontal sections of the synthetic model with a purely susceptible body. Panels A and B show the true model and inverted amplitude of magnetization, respectively, with the white arrows showing the direction of the magnetization vectors. Panels C and D show the amplitudes of induced and remanent magnetization, respectively.*

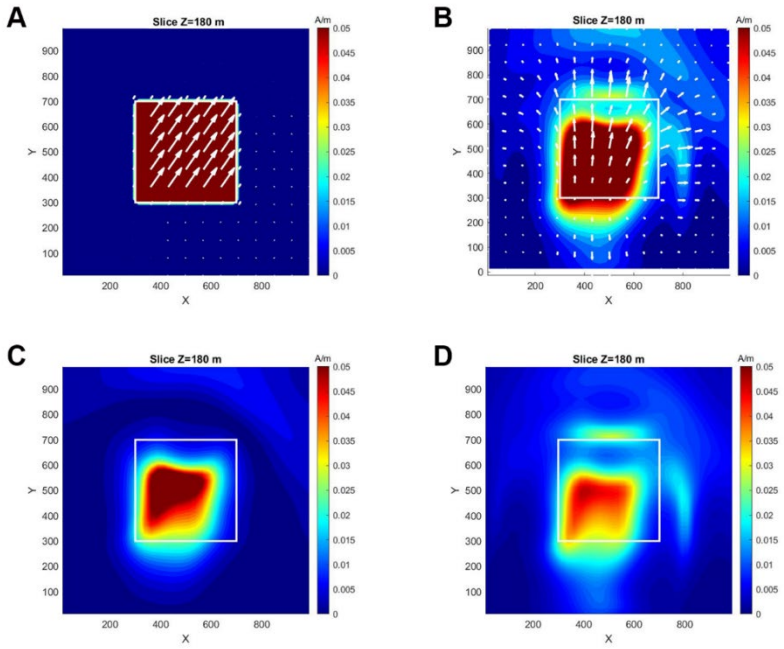

Figure 2 *Horizontal sections of the synthetic model with both induced and remanent components. Panels A and B show the true model and inverted amplitude of magnetization, respectively, with the white arrows showing the direction of the magnetization vectors. Panels C and D show the amplitudes of induced and remanent magnetization, respectively.*

Example from Nikka VMS
mineralization lens in McFaulds area of Ontario, Canada

The Nikka Volcanogenic Massive Sulfide (VMS) lens in the McFaulds area of Ontario, Canada is hosted in Archean mafic to felsic volcanic rocks with some sediments and igneous sills. As of 2020, there are inferred economic quantities of Cu (~2.5%), Au (~0.3 g/T), Ag (~7-8 g/T) and Zn (~2%) with a total tonnage of 500,000-850,000 (Geology Ontario, 2024). Pyrrhotite and magnetite concentrations are sufficient in the lens to generate a strong magnetic response. Figure 3 shows 3D models inverted from TMI data over the Nikka VMS lens. Panel A shows the location of the Ring of Fire complex in Ontario, Canada. Panel B presents the TMI data used in the inversions with the profile location shown by the white line. Panel C shows the inverted model obtained using a traditional method, which does not take remanence into account. We can see the VMS anomaly is apparently outcropping, which was not confirmed by the Spider Resources Inc. drill hole DDH McF-03-18 (Geology Ontario, 2024). Conversely, Panel D presents the inverted susceptibility model obtained using the new method of simultaneous inversion for susceptibility and remanence. The critical improvement in the new method is the clear delineation of the top of the VMS lens, which matched the drill hole log remarkably well.

Conclusions

The conventional algorithms focus solely on inverting the magnetic field to derive a magnetic susceptibility model. Conversely, the recently introduced Magnetization Vector Inversion (MVI) methods lack a comprehensive approach to accurately segregate the magnetization vector into induced and remanent magnetizations. This study introduces an innovative technique for inverting total magnetic intensity field data, enabling the simultaneous determination of magnetic susceptibility and induced and remanent magnetization. We tested this novel approach using synthetic models of magnetized bodies and data gathered over the Nikka VMS mineralization lens in the McFaulds area of Ontario, Canada. Directly reconstructing induced and remanent magnetization and recovering the magnetic susceptibility simultaneously with the remanent magnetization offers crucial geological and mineralization insights within the surveyed area.

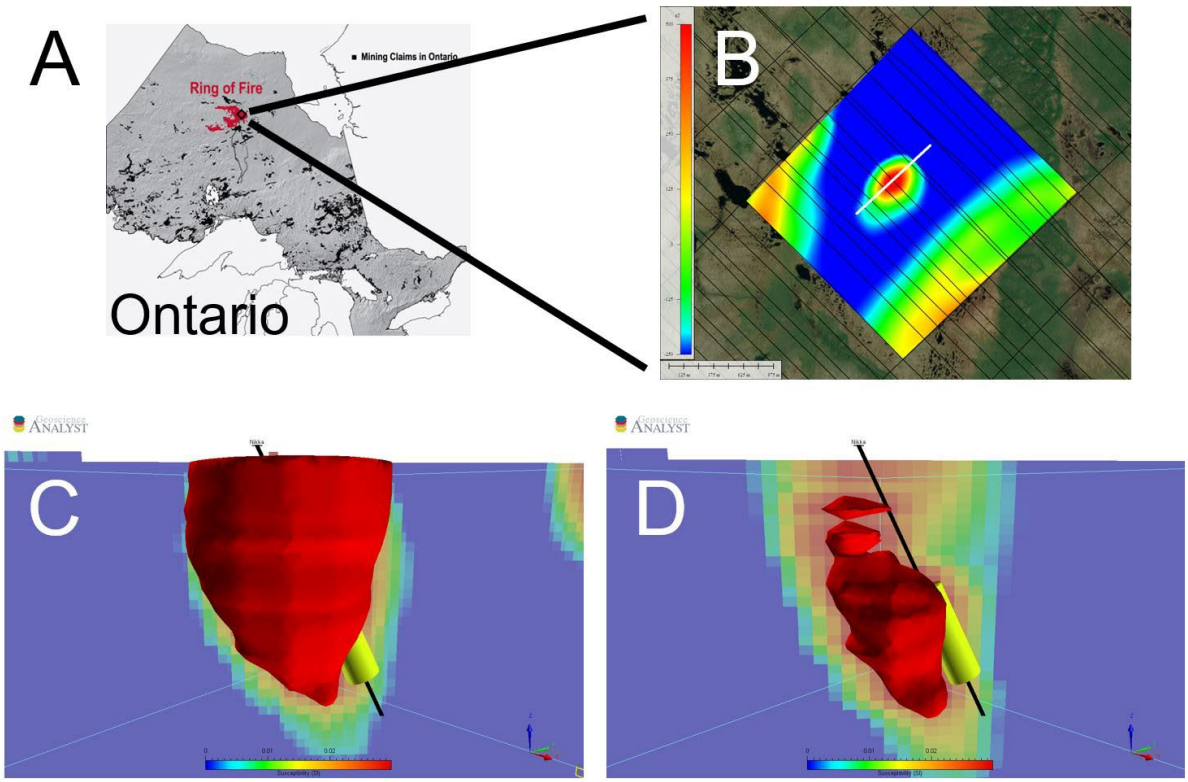

Figure 3 *Inversion of the TMI data over Nikka VMS in the McFaulds area of Ontario, Canada. The red isobodies in Panels C and D represent susceptibility values over 0.03 SI. The black line shows the drill hole and the green cylinder represents an interval with known VMS mineralization. The maximum susceptibility values in Panel C and D are ~0.04 SI and ~0.08 SI, respectively.*

Acknowledgments

The authors acknowledge the Consortium for Electromagnetic Modeling and Inversion (CEMI) at The University of Utah and TechnoImaging for the support of this research project.

References

Ellis, R. G., De Wet, B., and Macleod, I. N. [2012]. Inversion of magnetic data from remanent and induced sources. *22nd ASEG Geophysical Conference and Exhibition, Brisbane, Australia*, Expanded Abstracts.

Geology Ontario, "GeologyOntario – Ministry of Energy, Northern Development and Mines," accessed [2 Jan 2024], https://www.geologyontario.mndm.gov.on.ca/mndmfiles/mdi/data/records/MDI43D16SE00002.html.

Jorgensen, M., and Zhdanov, M. S. [2021]. Recovering magnetization of rock formations by jointly inverting airborne gravity gradiometry and total magnetic intensity data. *Minerals*, **11**, 366.

Jorgensen, M., Zhdanov, M. S., and Parsons, B. [2023]. 3D Focusing inversion of full tensor magnetic gradiometry data with Gramian regularization. *Minerals*, **13**, 851.

Li, Y. [2017]. From susceptibility to magnetization: advances in the 3D inversion of magnetic data in the presence of significant remanent magnetization. *Proceedings of Exploration 17: Sixth Decennial International Conference on Mineral Exploration*, 239--260.

Zhdanov, M. S. [2015]. *Inverse theory and applications in geophysics*. Elsevier.

Zhu, Y., Zhdanov, M. S., and Cuma, M. [2015]. Inversion of TMI data for the magnetization vector using Gramian constraints. *85th Annual International Meeting, SEG*, Expanded Abstracts, 1602-1606.